Physica E 53 (2013) 186–192

Contents lists available at SciVerse ScienceDirect

Physica E

journal homepage: www.elsevier.com/locate/physe

Resonant tunneling and enhanced Goos–Hänchen shift in a graphene double velocity barrier structure

Y. Wang [a], Y. Liu [b], B. Wang [a,*]

[a] School of Physics and Engineering, Sun Yat-sen University, 510275 Guangzhou, China
[b] School of Engineering, Sun Yat-sen University, 510275 Guangzhou, China

HIGHLIGHTS

- Transmission for Dirac fermions through graphene DVBs exhibits strong resonant tunneling effect.
- The resonant tunneling arises from Fabry–Pérot resonance and leads to oscillated conduction at wide energy range.
- Multi-GH shift peaks with giant magnitudes occur in graphene DVBs without the limits of transmission gap.

GRAPHICAL ABSTRACT

Graphene DVBs exhibits strong resonant tunneling effect and has multi giant GH shift peaks at wide energy range without the limits of transmission gap.

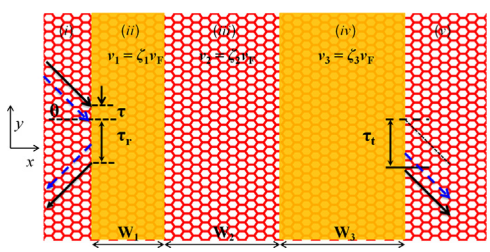

ARTICLE INFO

Article history:
Received 1 March 2013
Received in revised form
8 May 2013
Accepted 9 May 2013
Available online 21 May 2013

Keywords:
Resonant tunneling
Goos–Hänchen shift
Velocity barrier
Graphene

ABSTRACT

Resonant transmission and Goos–Hänchen (GH) shift for Dirac fermion beams tunneling through graphene double velocity barrier structures (DVBs) are investigated theoretically. Analytical and numerical results demonstrate that strong resonant tunneling effect occurs in this structure and is highly dependent on the incident angle and the structure of velocity barriers. The resonant tunneling in graphene DVBs belongs to the Fabry–Pérot resonance and leads to oscillated conduction at wide energy range. It is also found that GH shifts in this structure can be enhanced by the resonant tunneling and multi-GH shift peaks with giant magnitudes can occur at these resonant energy positions. These special properties of GH shifts in graphene DVBs may have good application in lateral manipulation of electron beams and valley or spin beam splitter.

1. Introduction

Since the successful fabrication of graphene [1], manipulating Dirac fermions in this material by external fields has aroused increasing attention owing to the effect of external fields on its line dispersion [2,3]. Besides geometric constraints, electric field, magnetic field and strain effect, inhomogeneous velocity profiles are recently used to manipulate Dirac fermions in graphene-based structures [4–11]. Generally, if a channel is close to or connected to a contact the Hamilton will exhibit modification viewed as the self-energy related to many-body interaction. Therefore, the conduction and valence bands of quasiparticle in this region under the contact will be renormalized and the quasiparticle velocity will be renormalized too. Similarly, a grounded metal plane close to graphene as a channel will also renormalize the Fermi velocity in corresponding graphene regions [4]. In addition, the group velocity in strained graphene can be changed owing to the deformation and shift of Dirac cones under strain [5]. It is also shown that the periodic potential with some specific patterns in graphene can renormalize group velocity by producing extra anisotropic Dirac cones [6,7]. All these methods changing and controlling the velocity provide an attractive route to velocity

* Corresponding author. Tel.: +86 20 8411 5692; fax: +86 20 8411 3293.
E-mail address: bwang6367@gmail.com (B. Wang).

1386-9477/$ - see front matter © 2013 Elsevier B.V. All rights reserved.
http://dx.doi.org/10.1016/j.physe.2013.05.010

barrier in graphene. On the other hand, the effective Hamiltonian in graphene with a position-dependent velocity distribution has been deduced by Peres [8]. In addition, the electronic transport through some velocity-modulated graphene nanostructures has been investigated, such as a velocity barrier and superlattice [9–11]. Some special properties in these velocity-modulated structures are demonstrated, including strong anisotropic transmission and tunneling [4,9], electron beam collimation [10] and disorder-corrected conductance fluctuations [11].

Electronic transmission through graphene double electrostatic potential barriers (DPBs) has been investigated and exhibits strongly resonant tunneling effect [12–16], which plays an important role on the quantum interference in graphene-based nanostructure [17–20] and has possibly potential applications in graphene-based devices with the ultrahigh proceeding speed. Motivated by the importance of the resonant tunneling effect and the special transport properties in velocity-modulated graphene structures, in this paper, we will present the resonant tunneling in graphene double velocity barrier structures (DVBs). In detail, we will evaluate the effect of the energy gap, the incident direction and the structures of double velocity barriers on the resonant tunneling.

Owing to the similarity between the Dirac-Weyl equation for Dirac fermions and the Helmholtz equation for light, Dirac fermions in graphene-based structures exhibit analogous light phenomena [21–23]. An important analogy is the Goos–Hänchen (GH) shift, which is referred to a lateral shift between the reflected beam and the incident beam at the interface between two optical materials with different refraction index on total internal reflection [24,25]. It has been figured out that the reflected and transmitted Dirac fermion beams in graphene potential barrier, strained barrier, velocity-modulated potential barrier and magnetic barrier exhibit obvious quantum Goos–Hänchen effect [26–33]. The quantum GH shift plays an important role on the manipulation of Dirac fermions in graphene and provides an important path for achieving valley or spin splitters. Recently, quantum GH shifts for Dirac fermions in graphene DPBs and double magnetic barriers (DMBs) have been investigated [31,33]. It is indicated that single giant GH shift peak in graphene DPBs appears inside the transmission gap [31]. Owing to the difference between the electrostatic potential barrier and velocity barrier, the transmission (reflection) through graphene velocity barrier structure is different from that through graphene electrostatic potential barrier, and hence the quantum GH shifts in graphene DVBs may exhibit some quite different behaviors. In this paper, we will present the GH shift in graphene DVBs. It is found that GH shift can be enhanced by the resonant tunneling and multi shift peaks of giant magnitude occur in graphene DVBs.

2. Theory formula

For the graphene-based medium, where a energy gap Δ is induced by symmetry breaking or spin–orbit interaction and Fermi velocity v varies in coordinate space as a function $v=v(\mathbf{r})$ of position vector $\mathbf{r}$, the massless Dirac–Weyl model is given by [4,8]

$$-i\hbar\sqrt{v(\mathbf{r})}\ \boldsymbol{\sigma}\cdot\nabla_{\mathbf{r}}\left[\sqrt{v(\mathbf{r})}\boldsymbol{\psi}(\mathbf{r})\right]+\Delta\boldsymbol{\sigma}_z\boldsymbol{\psi}(\mathbf{r})=E\ \ \boldsymbol{\psi}(\mathbf{r}) \tag{1}$$

where $\boldsymbol{\sigma}=(\boldsymbol{\sigma}_x, \boldsymbol{\sigma}_y)$, and $\boldsymbol{\sigma}_x$, $\boldsymbol{\sigma}_y$ and $\boldsymbol{\sigma}_z$ are the Pauli spin matrices, and $\boldsymbol{\psi}(\mathbf{r})=[\psi_A(\mathbf{r}), \psi_B(\mathbf{r})]^T$ is the two-component wave function. It is assumed that the velocity variation in this model is slow enough on the scale of the lattice constant. Taking into account the conservation of the momentum along y direction for the graphene DVBs in Fig. 1, we can conveniently introduce an auxiliary spinor $\boldsymbol{\Phi}(\mathbf{r})=\sqrt{v(x)}\boldsymbol{\psi}(x)e^{ik_y y}$ and further reduce Eq. (1) as the following form

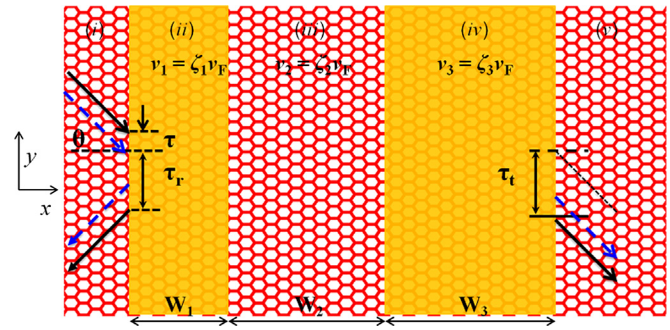

Fig. 1. Schematic diagram of the graphene DVBs with the yellow-shaded regions denoting the velocity barrier regions. The upper (solid line) and lower (dash line) components have a relative displacement τ.

$$-i\hbar v(x)(\partial_x\mp k_y)\Phi_{A(B)}(x)=(E\pm\Delta)\ \ \Phi_{B(A)}(x) \tag{2}$$

For the j region [$j=(i)$, (ii), (iii), (iv) or (v)] in Fig. 1 with Fermi velocity v_j, Eq. (2) can be further rewritten as

$$\frac{d^2}{dx^2}\Phi^j_{A(B)}(x)+\left[\frac{(E+\Delta)(E-\Delta)}{\hbar^2 v_j^2}-k_y^2\right]\Phi^j_{A(B)}(x)=0 \tag{3}$$

Using Eqs. (2) and (3), we can obtain the wave functions for Dirac fermions in any one of five regions in graphene DVBs, as follows:

For region (i),

$$\boldsymbol{\Phi}^{(i)}(x,y)=\begin{bmatrix} e^{ik_x x} & e^{-ik_x x}\\ s\beta e^{i\theta}e^{ik_x x} & -s\beta e^{-i\theta}e^{-ik_x x}\end{bmatrix}\begin{bmatrix}1\\ r\end{bmatrix}e^{ik_y y}=\mathbf{M}_1(x)\begin{bmatrix}1\\ r\end{bmatrix}e^{ik_y y} \tag{4}$$

For region (ii),

$$\boldsymbol{\Phi}^{(ii)}(x,y)=\begin{bmatrix} e^{iq_1 x} & e^{-iq_1 x}\\ s\beta e^{i\theta_1}e^{iq_1 x} & -s\beta e^{-i\theta_1}e^{-iq_1 x}\end{bmatrix}\begin{bmatrix}a_1\\ b_1\end{bmatrix}e^{ik_y y}=\mathbf{M}_2(x)\begin{bmatrix}a_1\\ b_1\end{bmatrix}e^{ik_y y} \tag{5}$$

For region (iii),

$$\boldsymbol{\Phi}^{(iii)}(x,y)=\begin{bmatrix} e^{ik_x x} & e^{-ik_x x}\\ s\beta e^{i\theta}e^{ik_x x} & -s\beta e^{-i\theta}e^{-ik_x x}\end{bmatrix}\begin{bmatrix}c\\ d\end{bmatrix}e^{ik_y y}=\mathbf{M}_3(x)\begin{bmatrix}c\\ d\end{bmatrix}e^{ik_y y} \tag{6}$$

For region (iv),

$$\boldsymbol{\Phi}^{(iv)}(x,y)=\begin{bmatrix} e^{iq_2 x} & e^{-iq_2 x}\\ s\beta e^{i\theta_2}e^{iq_2 x} & -s\beta e^{-i\theta_2}e^{-iq_2 x}\end{bmatrix}\begin{bmatrix}a_2\\ b_2\end{bmatrix}e^{ik_y y}=\mathbf{M}_4(x)\begin{bmatrix}a_2\\ b_2\end{bmatrix}e^{ik_y y} \tag{7}$$

For region (v),

$$\boldsymbol{\Phi}^{(v)}(x,y)=\begin{bmatrix} e^{ik_x x} & e^{-ik_x x}\\ s\beta e^{i\theta}e^{ik_x x} & -s\beta e^{-i\theta}e^{-ik_x x}\end{bmatrix}\begin{bmatrix}t\\ 0\end{bmatrix}e^{ik_y y}=\mathbf{M}_5(x)\begin{bmatrix}t\\ 0\end{bmatrix}e^{ik_y y} \tag{8}$$

In Eqs. (4)–(8), $s=\text{sign}(E)$, $\beta=\hbar v_F k/(E+\Delta)$ with $k^2=(E^2-\Delta^2)/(\hbar v_F)^2$, $k_x=\sqrt{k^2-k_y^2}$, $q_1=\sqrt{k^2/\zeta_1^2-k_y^2}$, $q_2=\sqrt{k^2/\zeta_2^2-k_y^2}$, $\theta=\arctan(k_y/k_x)$, $\theta_1=\arctan(k_y/q_1)$ and $\theta_2=\arctan(k_y/q_2)$. Obviously, there is $\mathbf{M}_1=\mathbf{M}_3=\mathbf{M}_5$ in Eqs. (4), (6) and (8). By using the continuity of wave functions at left (L) and right (R) boundaries of any velocity interface, we can obtain

$$\begin{bmatrix} 1 \\ r \end{bmatrix} = \mathbf{M}\begin{bmatrix} t \\ 0 \end{bmatrix} = \begin{bmatrix} M_{11} & M_{12} \\ M_{21} & M_{22} \end{bmatrix}\begin{bmatrix} t \\ 0 \end{bmatrix} \tag{9}$$

$$\mathbf{M} = \mathbf{M}_1{}^{-1}(\mathrm{R})\mathbf{M}_2(\mathrm{L})\mathbf{M}_2{}^{-1}(\mathrm{R})\mathbf{M}_3(\mathrm{L})\mathbf{M}_3{}^{-1}(\mathrm{R})\mathbf{M}_4(\mathrm{L})\mathbf{M}_4{}^{-1}(\mathrm{R})\mathbf{M}_5(\mathrm{L}) \tag{10}$$

According to Eqs. (9) and (10), the reflection coefficient r and the transmission coefficient t are obtained by

$$r(k_y) = \left|r(k_y)\right|\exp\left[i\mu_r(k_y)\right] = M_{21}/M_{11} \tag{11}$$

$$t(k_y) = \left|t(k_y)\right|\exp\left[i\mu_t(k_y)\right] = 1/M_{11} \tag{12}$$

where $\mu_r(k_y)$ is the reflection phase and $\mu_t(k_y)$ is the transmission phase.

The stationary-phase approximation shows that the GH shifts of reflected (transmitted) beam result from the negative gradient of the reflection (transmission) phase in direction [25]. Owing to the pseudospin of Dirac fermions, the upper (+) and lower (−) components of reflected (transmitted) beam have their corresponding lateral shifts, which can be written as

$$\tau_r^{\pm} = -d\mu_r/dk_{y0} \mp \tau \tag{13}$$

$$\tau_t^{\pm} = -d\mu_t'/dk_{y0} \mp \tau \tag{14}$$

where τ is the relative displacement between upper and lower components of the incident beam, subscript 0 in these expressions denotes the values taken at $k_y = k_{y0}$ and $\mu_t' = \mu_t + q_1W_1 + k_xW_2 + q_3W_3$ is the total transmission phase [33]. Usually, the average shifts $\tau_{r,\ t} = (\tau_{r,\ t}^{+} + \tau_{r,\ t}^{-})/2$ are used to denote the GH shifts. Owing to $k_y = E/\hbar v_F \sin\ \theta = k_F \sin\ \theta$, $d\mu_r/dk_y$ and $d\mu_t/dk_y$at incident angle θ can be rewritten as

$$d\mu_r/dk_y = \frac{1}{k_F \cos\ \theta} d\mu_r/d\theta$$

$$d\mu_t/dk_y = \frac{1}{k_F \cos\ \theta} d\mu_t/d\theta$$

Therefore, the GH shifts in Eqs. (13) and (14) can also be rewritten as

$$\tau_r k_F = -\frac{1}{\cos\ \theta} d\mu_r/d\theta \tag{15}$$

$$\tau_t k_F = -\frac{1}{\cos\ \theta} d\mu_t'/d\theta \tag{16}$$

Because the average shift is used to denote the GH shift, the reflected and transmitted GH shifts are independent of the relative displacement τ between upper and lower components. In other words, it is not necessary to require τ in Eqs. (13)–(16).

In order to compare with graphene double velocity barriers, we also consider single graphene velocity barrier with width W and magnitude ζv_F. By using the continuity of wave functions at the boundaries, we can easily obtain the reflection coefficient r and the transmission coefficient t

$$r = \left|r\right|\exp(i\mu_r) = \frac{\sin(qW)(\sin\ \theta - \sin\theta')(\cos\ \theta + i\sin\ \theta)}{\cos(qW)\cos\ \theta\cos\theta' + i\sin(qW)(\sin\ \theta\sin\theta' - 1)} \tag{17}$$

$$t = \left|t\right|\exp(i\mu_t) = \frac{\cos\ \theta\cos\theta'}{\cos(qW)\cos\ \theta\cos\ \theta' + i\sin(qW)(\sin\ \theta\sin\theta' - 1)} \tag{18}$$

where θ and θ' are the incident and refraction angles, respectively, and $q = (k_F{}^2/\zeta^2 - k_y{}^2)^{1/2}$ with $k_F = E/\hbar v_F$ is the x component of wavevector in the barrier region. According to Eqs. (17) and (18), the reflection and transmission phases can be obtained by

$$\mu_r = \theta - \arctan\left[\frac{\sin(qW)(\sin\ \theta\sin\theta' - 1)}{\cos(qW)\cos\ \theta\cos\theta'}\right] \tag{19}$$

$$\mu_t = \arctan\left[\frac{\sin(qW)(\sin\ \theta\sin\theta' - 1)}{\cos(qW)\cos\ \theta\cos\theta'}\right] \tag{20}$$

Because the resonant tunneling peaks with perfect transmission in graphene single velocity or DVBs require electron to transmit perfectly through these barriers, i.e., $t=1$ or $r=0$ ($qW = n\pi$) in Eqs. (17) and (18) for any one barrier. Therefore, the resonant condition in graphene DVBs is given by $q_1W_1 = q_3W_3 = n\pi$, where n is an integer value. Owing to q_1 and q_3 as the longitudinal wave vector in first and second velocity barriers in graphene DVBs, the resonant condition can be rewritten as

$$\sqrt{(E^2-\Delta^2)/(\zeta_1\hbar v_F)^2 - k_y^2}\ W_1 = \sqrt{(E^2-\Delta^2)/(\zeta_3\hbar v_F)^2 - k_y^2}\ W_3 = n\pi \tag{21}$$

3. Results and discussion

3.1. Resonant tunneling through a graphene DVBs

Fig. 2 shows a few contour plots of transmission probability T ($T = \left|t\right|^2$) of electrons through graphene DVBs. Symmetric and asymmetric structures are used: $W_1 = W_3 = 50$ nm and $\zeta_1 = \zeta_3 = 0.5$ for the symmetric structure; $W_1 = 30$ nm, $W_3 = 70$ nm and $\zeta_1 = \zeta_3 = 0.5$ for the asymmetric structure induced by widths of barrier and $W_1 = W_3 = 50$ nm, $\zeta_1 = 0.3$ and $\zeta_3 = 0.7$ for the asymmetric structure induced by the magnitudes of barrier; and in all cases $W_2 = 100$ nm and $\zeta_2 = 1$. Compared with the transmission in Fig. 2(a), the forbidden region of transmission in Fig. 2(b) obviously exists near the zero energy owing to the energy gap. In the case of $\Delta = 0$ meV, the transmissions at small incident angle are nearly perfect as shown in Fig. 2(a), (c) and (d), which is a typical transmission feature for graphene-based structures [12–14,34]. One remarkable result indicates that the transmissions exhibit highly resonant and anisotropic behaviors in all these structures. From Fig. 2(a), (c) and (d), it can also be observed that the resonant tunneling exists inside the whole energy range and there is no transmission gap. Usually, a transmission gap occurs if total internal reflection (TIR) angle θ_c can be equal to zero, because the transmission gap forbids transmission in all directions. It has been demonstrated that in graphene electrostatic barrier structure a transmission gap can happen at $E = V$ [13], where V is the potential magnitude, since $\theta_c = \arcsin\left[(E-V)/E\right]$ is equal to zero at $E = V$. However, the TIR angle $\theta_c = \arcsin\left[\zeta_L/\zeta_R\right]$ is impossibly equal to zero in graphene velocity barrier, with left and right velocities $\zeta_L v_F$ and $\zeta_R v_F$ at the velocity barrier interface, respectively. Therefore, there is no transmission gap in graphene velocity barrier. As a result, at the incident interface in Fig. 2(a), there is $\zeta_L = 1$, $\zeta_R = 0.5$ and $\theta_c = \arcsin(2)$. This means that incident electron in any direction can transmit, which is similar to the light from a denser medium into a thinner one. In other words, there are no bound states in our graphene DVB structure with $\zeta_1 < 1$ and $\zeta_3 < 1$. Therefore, the resonant tunneling in graphene DVB results from the typical Fabry–Pérot resonance and is never related to transmission gap as well as bound states. It should be mentioned that velocity barriers with $\zeta_1 > 1$ and $\zeta_3 > 1$ should be considered, but calculated results show that the resonant transmission in this situation is weak. Hence, we only pay attention to the double velocity barriers with $\zeta_1 < 1$ and $\zeta_3 < 1$.

Fig. 3 further shows the transmission probability as a function of incident angle at some specific incident energies. It can be seen that the perfect transmission is suppressed with energy gap and the resonance is obviously enhanced with increasing the incident

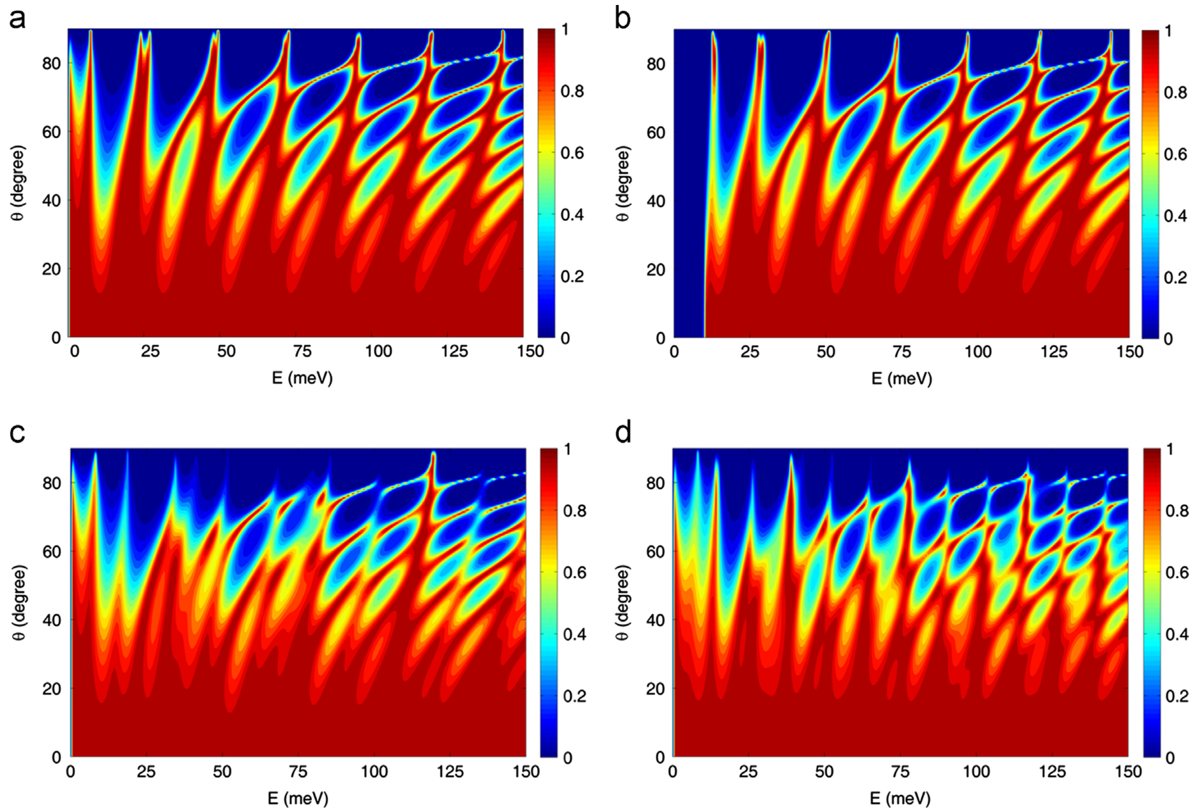

Fig. 2. Contour plots of transmission probability T as a function of energy E and angle θ. (a) $W_1=W_3=50$ nm, $\zeta_1=\zeta_3=0.5$ and $\Delta=0$ meV. (b) $W_1=W_3=50$ nm, $\zeta_1=\zeta_3=0.5$ and $\Delta=10$ meV. (c) $W_1=30$ nm, $W_3=70$ nm, $\zeta_1=\zeta_3=0.5$ and $\Delta=0$ meV. (d) $W_1=W_3=50$ nm, $\zeta_1=0.3$, $\zeta_3=0.7$ and $\Delta=0$ meV. In all cases $W_2=100$ nm and $\zeta_2=1$. (For interpretation of the references to color in this figure legend, the reader is referred to the web version of this article.)

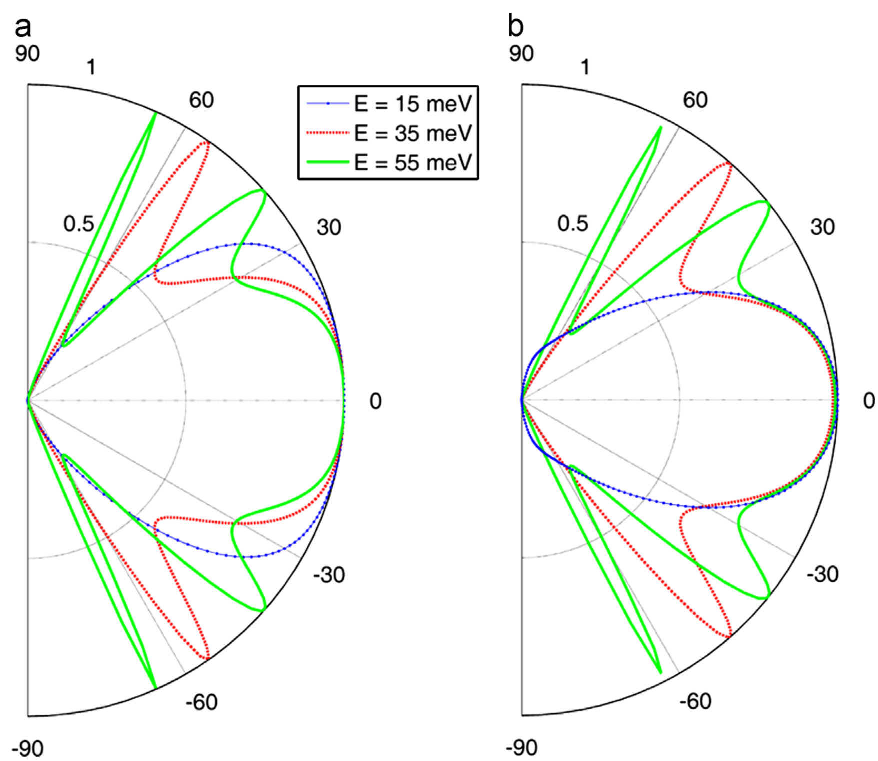

Fig. 3. Angular dependence of the transmission probability (T), for different values of energy (E). The physical parameters are identical to those in Fig. 2(a) and (b). (For interpretation of the references to color in this figure legend, the reader is referred to the web version of this article.)

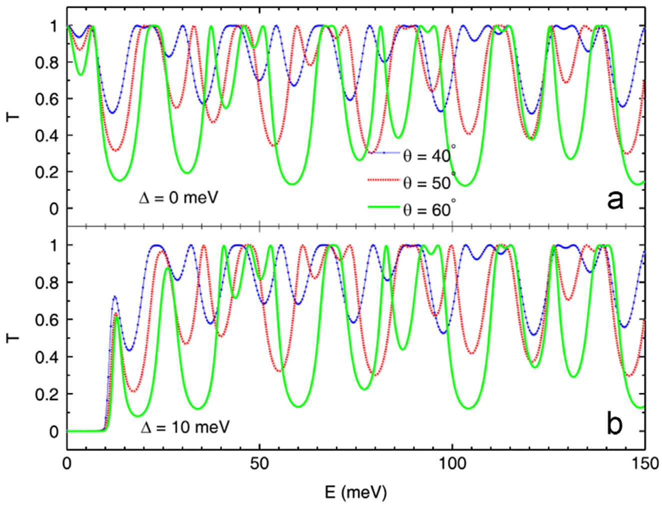

Fig. 4. Transmission probability (T) as a function of energy (E) at different incident angles. The physical parameters are identical to those in Fig. 2(a) and (b). For interpretation of the references to color in this figure legend, the reader is referred to the web version of this article.)

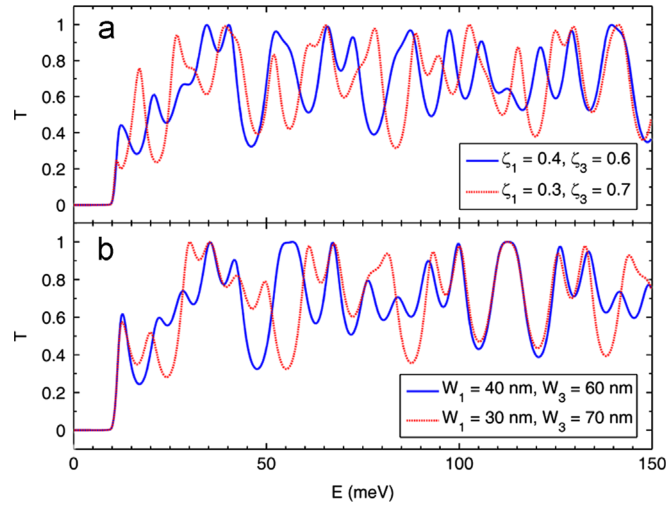

Fig. 5. Transmission probability (T) as a function of energy (E) for different widths and magnitudes of barriers with $\theta=50^\circ$. (a) $W_1=W_3=50$ nm, $\Delta=10$ meV. (b) $\zeta_1=\zeta_3=0.5$ and $\Delta=10$ meV. In all cases $W_2=100$ nm and $\zeta_2=1$. (For interpretation of the references to color in this figure legend, the reader is referred to the web version of this article.)

energy. Fig. 4 shows the transmission probability as a function of incident energy at some specific incident angles. The resonant transmission is enhanced with increasing the incident angle and the resonant energy locations of peaks satisfy the resonant condition in Eq. (21). On the other hand, the resonant condition also shows that the resonant tunneling is obviously dependent on the widths and magnitudes of two barriers, energy gap and the energy of incident electron. As shown in Fig. 5, the widths and magnitudes of two barriers have an obvious influence on the resonant transmission. Although the resonant condition is consistent between DPBs and DVBs, there is an obvious difference on the resonant tunneling. For graphene DPBs, the resonant tunneling peak happens inside the transmission gap at nonzero incidence angle since the bound states only occurs inside the transmission gap [13]. For graphene DVBs, the resonant tunneling peak appears at some specific energy positions without limits of transmission gap, due to the Fabry–Pérot resonance, as shown in Figs. (2), (4) and (5).

In order to evaluate the effect of the resonant tunneling on the conductance in graphene DVBs, we calculate the angularly averaged conductance by using $G=G_0\int_{-\pi/2}^{\pi/2}T(E,E\sin\,\theta)E\cos\,\theta d\theta$ with $G_0=2e^2L_y/h^2v_F$ and L_y as the sample size along the y direction [18], and plot the results in Fig. 6. Note that forbidden region of conduction near zero energy is enhanced with increasing the energy gap, as presented by the inset in Fig. 6. More importantly, the conductance exhibits oscillations induced by the resonant tunneling through the graphene DVBs. Different from the oscillated conductance appearing inside the transmission gap for graphene DPBs, the oscillated conductance happens inside the whole energy range for graphene DVBs. The wide energy range of oscillated conduction may have good application in quantum interference based on graphene-based nanostructure [17–20].

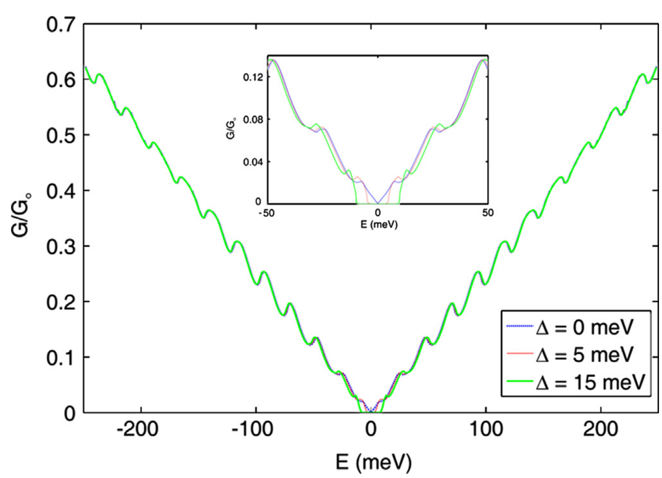

Fig. 6. Conduction as a function of energy (E) for different energy gap with $\zeta_1=\zeta_3=0.5$, $W_1=W_3=50$ nm, $W_2=100$ nm and $\zeta_2=1$. The inset shows the conduction for energy from −50 meV to 50 meV. (For interpretation of the references to color in this figure legend, the reader is referred to the web version of this article.)

3.2. Goos-Hänchen shift in graphene DVBs

Fig. 7 shows the GH shift as a function of Fermi energy at some specific incident angles, where structure parameters are chosen as $\zeta_1=\zeta_3=0.5$, $W_1=W_3=50$ nm, $W_2=100$ nm, $\zeta_2=1$ and $\Delta=0$ meV. It can be observed the GH shifts in graphene DVBs have obvious peaks and these peaks are enhanced by increased incident angles. According to the analytical expression of GH shifts in Eqs. (15) and (16), the dependence of GH shifts on the incident angle is the reciprocal of cosine function for angle. Therefore, the greater the incident angle is, the bigger the GH shifts are. In addition, as shown in Fig. 7, the energy locations of these peaks for GH shifts are exactly corresponding to those of resonant transmission in graphene DVBs. Owing to the Fabry–Pérot resonant condition, only electron beams with incident energy near the resonant energy positions can transmit through the graphene DVBs. In other words, electron beams with energies deviating from the resonant energy locations are reflected totally and exhibit usual GH shifts. Therefore, only these electron beams satisfying the resonant condition in Eq. (21) exhibit unusually enhanced GH shifts due to the Fabry–Pérot resonance. Thus, these enhanced GH shift peaks are corresponding to the tunneling peaks.

On the other hand, the resonant condition in Eq. (21) also indicates the Fabry–Pérot resonance in graphene DVB is dependent on width and magnitude of velocity barrier. Therefore, the GH shifts will also rely on the barrier width and magnitude. Fig. 8 shows the GH shift as a function of Fermi energy with different widths and magnitudes of barriers, respectively. Obviously, the GH

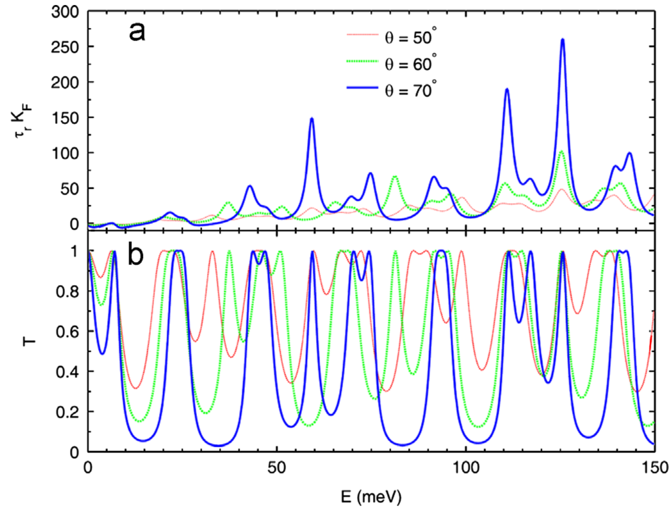

Fig. 7. The GH shift as a function of energy at some specific incident angles with $\zeta_1=\zeta_3=0.5$, $W_1=W_3=50$ nm, $W_2=100$ nm, $\zeta_2=1$ and $\Delta=0$ meV. (a) The GH shift of reflected beams. (b) Corresponding transmission probability. (For interpretation of the references to color in this figure legend, the reader is referred to the web version of this article.)

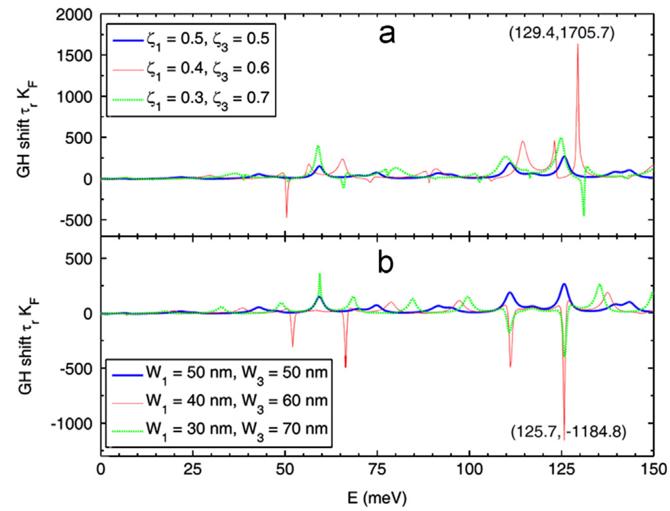

Fig. 8. The GH shift as a function of energy for different widths and magnitudes of barriers with $\theta=70°$. (a) $W_1=W_3=50$ nm, $\Delta=0$ meV. (b) $\zeta_1=\zeta_3=0.5$ and $\Delta=0$ meV. In all cases $W_2=100$ nm and $\zeta_2=1$. (For interpretation of the references to color in this figure legend, the reader is referred to the web version of this article.)

shifts with enhanced magnitudes occur and are tuned by the barrier width and velocity magnitude and have positive or negative values. For example, the maximum of GH shift induced by velocity barrier magnitudes in Fig. 8(a) is 1705.7 at energy position 129.4 meV and the maximum magnitude of GH shift induced by barrier widths in Fig. 8(b) is 1184.8 but negative at energy position 125.7 meV. In fact, the electron beams in this Fabry–Pérot structure are subjected to multiple reflections and interferences leading to the bigger phase gradient in direction. In other words, owing to the Fabry–Pérot resonance, the multiple reflections and interferences reshape the electron wavepacket and induce the bigger phase gradient of electron wavepacket in the incident angle, which enhances the GH shift, as supported by Eqs. (15) and (16).

Although a previous work has shown that velocity can control the Goos–Hänchen shift of reflected electron beams at graphene p–n interface [32] and it is also shown that giant GH shifts can exist in graphene DPBs [31], there is remarkable difference on the enhanced GH shifts between DPBs and DVBs. The difference should be attributed to the different underlying physic mechanisms between DPBs and DVBs. The enhanced GH shifts in graphene DPBs arise from the bound states inside the transmission gap [31]. However, in this present work, the enhanced GH shift with giant magnitude in graphene DVBs origins from the Fabry–Pérot resonance, which reshapes electron wavepacket and induces the bigger phase gradient in direction. As long as the energy of incident electron at a greater incident angle satisfies the resonant condition in Eq. (21), these incident electron beams will exhibit enhanced GH shifts. Therefore, the enhanced GH shifts in graphene DVBs occur at wide energy range without the limits of the transmission gap. Owing to multi-resonant energy positions satisfying the resonant condition, multi-GH shift peaks with giant magnitudes occur. These enhanced GH shift peaks may strengthen the ability of application in valley or spin beam splitters, which require GH shifts of electron beams to have large magnitude in order to effectively split the valley or spin electron beams [29,35].

4. Conclusion

In summary, we have investigated the transmission and GH shift for Dirac fermions through graphene DVBs. The transmission exhibits strong resonant behaviors and relies on the induced energy gap, widths and magnitudes of double barriers and the incident angle. The resonant tunneling is a direct consequence of Fabry-Pérot resonance and leads to oscillated conduction at wide energy range, which may have potential application in quantum interference based on graphene-based devices. The GH shifts in graphene DVBs are obviously enhanced up to giant magnitude and these enhanced GH shift peaks are corresponding to the tunneling peaks, owing to the Fabry–Pérot resonance inducing the bigger phase gradient in direction at these resonant energy locations. Therefore, different from single giant GH shift peak inside the transmission gap in graphene DPBs, multi-GH shift peaks with giant magnitudes occur in graphene DVBs without the limits of transmission gap. These special properties of GH shifts in graphene DVBs may have potential application in valley or spin beam splitter based on the graphene-based nanostructure.

To achieve the real spin or valley splitter with obvious splitting distance, in the near future, we will further present the spin- and valley-dependent giant GH shifts in the presence of the Zeeman interaction under magnetic field [36], spin–orbit interaction [37,38], or local strain effect [5,39].

Acknowledgement

This work was supported by the NSFC (Nos. 10902128, 10732100 and 11072271).

References

[1] K.S. Novoselov, A.K. Geim, S.V. Morozov, D. Jiang, Y. Zhang, S.V. Dubonos, I. V. Grigorieva, A.A. Firsov, Science 306 (2004) 666.
[2] A.H. Castro Neto, F. Guinea, N.M.R. Peres, K.S. Novoselov, A.K. Geim, Reviews of Modern Physics 81 (2009) 109.
[3] D.S.L. Abergel, V. Apalkov, J. Berashevich, K. Ziegler, T. Chakraborty, Advances in Physics 59 (2010) 261.
[4] A. Raoux, M. Polini, R. Asgari, A.R. Hamilton, R. Fazio, A.H. MacDonald, Physical Review B: Condensed Matter **81** (2010) 073407.
[5] F.M.D. Pellegrino, G.G.N. Angilella, R. Pucci, Physical Review B: Condensed Matter 84 (2011) 195404.
[6] M. Barbier, P. Vasilopoulos, F.M. Peeters, Physical Review B: Condensed Matter 81 (2010) 075438.
[7] C.-H. Park, L. Yang, Y.-W. Son, M.L. Cohen, S.G. Louie, Nature Physics **4** (2008) 213.
[8] N.M.R. Peres, Journal of Physics: Condensed Matter 21 (2009) 095501.

[9] A. Concha, Z. Tešanović, Physical Review B: Condensed Matter **82** (2010) 033413.
[10] P.M. Krstajić, P. Vasilopoulos, Journal of Physics: Condensed Matter **23** (2011) 135302.
[11] A. Esmailpour, H. Meshkin, R. Asgari, Solid State Communications 152 (2012) 1896.
[12] J. Milton Pereira Jr., P. Vasilopoulos, F.M. Peeters, Applied Physics Letters **90** (2007) 132122.
[13] R. Zhu, Y. Guo, Applied Physics Letters **91** (2007) 252113.
[14] C. Bai, Y. Yang, X. Zhang, Physical Review B: Condensed Matter 80 (2009) 235423.
[15] M. Dragoman, D. Dragoman, G. Deligiorgis, G. Konstantinidis, D. Neculoiu, A. Cismaru, R. Plana, Journal of Applied Physics 106 (2009) 044312.
[16] R. Biswas, S. Mukhopadhyay, C. Sinha, Physica E: Low-dimensional Systems and Nanostructures 42 (2010) 1781.
[17] A.V. Shytov, M.S. Rudner, L.S. Levitov, Physical Review Letters 101 (2008) 156804.
[18] M. Ramezani Masir, P. Vasilopoulos, F.M. Peeters, Physical Review B: Condensed Matter 82 (2010) 115417.
[19] A.F. Young, P. Kim, Nature Physics 5 (2009) 222.
[20] J. Velasco Jr., G. Liu, W. Bao, C.N. Lau, New Journal of Physics 11 (2009) 095008.
[21] V.V. Cheianov, V. Fal'ko, B.L. Altshuler, Science 315 (2007) 1252.
[22] S. Ghosh, M. Sharma, Journal of Physics: Condensed Matter **21** (2009) 292204.
[23] I. Mihalache, D. Dragoman, Journal of the Optical Society of America B: Optical Physics 28 (2011) 1746.
[24] F. Goos, H. Hänchen, Annals of Physics 436 (1947) 333.
[25] R.H. Renard, Journal of the Optical Society of America A: Optics, Image Science, and Vision **54** (1964) 1190–1196.
[26] C.W.J. Beenakker, R.A. Sepkhanov, A.R. Akhmerov, J. Tworzydło, Physical Review Letters 102 (2009) 146804.
[27] Z. Wu, F. Zhai, F.M. Peeters, H.Q. Xu, K. Chang, Physical Review Letters 106 (2011) 176802.
[28] M. Sharma, S. Ghosh, Journal of Physics: Condensed Matter **23** (2011) 055501.
[29] F. Zhai, Y. Ma, K. Chang, New Journal of Physics 13 (2011) 083029.
[30] X. Chen, J.-W. Tao, Y. Ban, European Physical Journal B: Condensed Matter and Complex Systems **79** (2011) 203.
[31] Y. Song, H.-C. Wu, Y. Guo, Applied Physics Letters 100 (2012) 253116.
[32] Y. Wang, Y. Liu, B. Wang, Physica E: Low-dimensional Systems and Nanostructures 48 (2013) 191.
[33] Y. Wang et al., Tunable electron wave filter and Goos–Hänchen shift in asymmetric graphene double magnetic barrier structures, Superlattices and Microstructure (2013), 〈http://dx.doi.org/10.1016/j.spmi.2013.04.035〉.
[34] M.I. Katsnelson, K.S. Novoselov, A.K. Geim, Nature Physics 2 (2006) 620–625.
[35] X. Chen, X.J. Lu, Y. Wang, C.F. Li, Physical Review B: Condensed Matter **83** (2011) 195409.
[36] L. Dell'Anna, A.De Martino, Physical Review B: Condensed Matter 80 (2009) 155416.
[37] P.M. Krstajić, P. Vasilopoulos, Physica E: Low-dimensional Systems and Nanostructures **42** (2010) 929.
[38] C. Bai, J. Wang, S. Yuan, Y. Yang, Physica E: Low-dimensional Systems and Nanostructures 43 (2010) 398.
[39] F. Guinea, M.I. Katsnelson, A.K. Geim, Nature Physics **6** (2010) 30.